DEVELOPMENT OF A CEMS PLATFORM BASED ON MUMPS PROCESS

N. Scuor[a], P. Gallina[b], M. Nicolich, O. Sbaizero[a], and V. Sergo[a]

[a] CENMAT – Center of Excellence for Nanostructured Materials, University of Trieste, 34127 Trieste, Italy
[b] Dipartimento di Ingegneria Meccanica, Università di Trieste, 34127 Trieste (Italy)

Abstract
First introduced at the University of Colorado, CEMS (Cellular Engineering Micro Systems) is an enabling technology and research platform for cellular research. By combining the engineering technology known as MEMS (MicroElectrical Mechanical Systems) and cellular biology, CEMS technology will allow researches to study individual cells.
A CEMS platform of novel type, based on the MUMPS process, has been designed and manufactured. It enables researcher to apply and measure stresses on a living single cell, in a biaxial fashion, while keeping the manufacturing costs low. Furthermore, the particular geometry of the linkages, which has been developed, results in a very predictable and reliable mechanical behaviour, and allows to use a very simple control system. The device has been designed and optimized using finite element analysis techniques. Moreover, an analytical model for the entire system has been developed and compared against the experimental data.

Keywords: MEMS, Cell stretching, Mechanical loading, Biaxial loading

1 INTRODUCTION

In the golden jubilee issue of Acta Materialia, which can probably be considered the forefather of the present journal, Van Vliet et al. traced an exhaustive survey of the tools available to researchers in the biomechanics machine-shop. It is the purpose of this contribution to present a new tool, which can be used for the mechanical stimulus of cells. Stress/strain (and load/displacement) can profoundly effect the behaviour of cells, as has been comprehensively described by Fung in several contributions [1-3]. Whereas the uniaxial loading configuration has been described and used successfully in several cases [4-6], the biaxial stretching remains more elusive, since it is limited to the flexion of membranes [7-17]. Nevertheless, this load condition is common among cells present in tissues which play a key role in the human body, like, for example, the pericardium. Here a new Micro Electro Mechanical System (MEMS) is described, which is based on the idea of in-plane biaxial stretching rather than out-of-plane stretching, typical of the flexion of membranes. Actually, there is a strong difference in the amplitude of the obtainable horizontal displacements in the two cases. In fact, the motion in a direction normal to the MEMS seating plane, can develop in-plane displacements limited to much less than one micron, if conventional manufacturing technologies, like the MUMPS one, are employed. In contrast to this, the in-plane motion can develop, as in the present case, some microns of in-plane displacement, with minor difficulties, using only flexural joints. This better compares with the dimensions of typical target cells, like adult myocytes, that can be of the order of 50 microns [14].

A picture of the device is presented in Figure 1. The circular, four quadrant sectioned plate constitutes the seating plane for the cell under test, which ideally should be positioned at the platform centre, after proper functionalization of the underlying surface. The focus of the present contribution is to provide a set of guidelines for the design, the manufacturing and the operation of a device for the mechanical characterization in the field of biomechanics. The paper will be organized as follows: section 2 will be devoted to materials and methods; section 3 will present results and discussion; Finally, section 4 will present some conclusions.

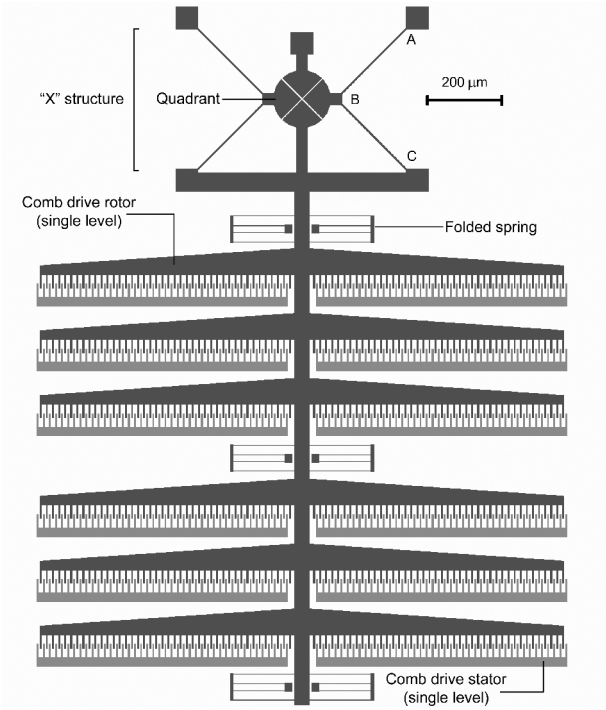

Figure 1: Layout of the biaxial MEMS cell stretcher.

2 MATERIALS AND METHODS

2.1 Device description

The equivalent kinematic scheme of the device is depicted in Figure 2. In fact, in order to gain an insight into the kinematic behaviour of the device, each beam which constitutes the cell stretcher is modeled by means of a rigid beam. Moreover rigid beams are linked one to the other by means of hinged joints, which take into account the on-plane compliance of the real beam. Figure 2 represents the right half of the upper part of the complete

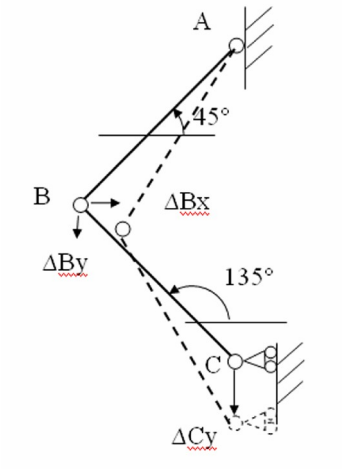

Figure 2: Kinematic principle of the MEMS device.

cell stretcher (Figure 1). Points A, B and C of Figure 2 correspond to the same points of Figure 1.

The heart of the cell stretcher is the set of 4 disc quadrants. The slide allows the vertical displacement of point C; point B represents the position of the right quadrant. Notice that beams are tilted respectively of 45° and 135° with respect to the horizontal in the undeformed configuration (see solid line mechanism). When a force is applied to the cell stretcher, causing a downward motion ΔC_y of point C, the point B moves towards the right and downwards, respectively of ΔB_x and ΔB_y (see dot line mechanism). If small displacements are assumed, it can be inferred that

$$\Delta B_x \cong \Delta C_y / 2 \qquad \Delta B_y = \Delta C_y / 2 \tag{1}$$

Such relationships are satisfied if and only if the two beams have same length and the angle they form is 90°. Therefore, considering the cell stretcher symmetry, the distance Δx and Δy between the tips of the horizontal and vertical quadrants are

$$\Delta x = \Delta x_0 + 2\Delta B_x \cong \Delta x_0 + \Delta C_y \qquad \Delta y = \Delta y_0 + 2\Delta B_y = \Delta y_0 + \Delta C_y \tag{2}$$

respectively, where Δx_0 and Δy_0 are tip distances in the undeformed configuration. Eq.s (2) do not hold for large displacements since nonlinearities occur; in particular, for high values of ΔC_y, ΔB_x tends to decrease with respect to ΔB_y. As it will be shown, for small displacements, both Finite Elements Analysis FEA and experimental results validate the initial assumptions.

Six folded springs are connected to the central bar of the vertical moving structure of the device. They are necessary to bring the bar back to its initial position once the driving voltage is switched off. Secondly, they prevent the comb drive from exhibiting lateral instability.

Exploiting the Saint-Venant linear beam theory [18], the spring stiffness can be calculated according to:

$$K_b = 24EJ / (I_1^3 + I_2^3) \tag{3}$$

where E is the Young's modulus, J is the moment of inertia, l_1 and l_2 are the lengths of the beams constituting the folded spring. Using the values listed in Table 1 the spring stiffness results 90.7 N/m. Moreover, the stiffness k of the 'X' structure, which is approximately 8 times the one of each single folded spring, can not be neglected. Its value has been estimated by means of FEA (see Figure 3). In conclusion, the total stiffness, which is the sum of the seven contributions, is 17.5 N/m.

Table 1: Phisical constants for stiffness evaluation.

DESCRIPTION	*SYMB.*	*VALUE*	*UNIT*
Young modulus	E	170	GPa
Moment of inertia	J	145.8	μm^4
Length of the long leg	l_1	160	μm
Length of the short leg	l_2	135	μm

Several actuation principles can be employed in order to operate the cell stretcher: thermal actuation, comb drive, magnetic actuation, piezoelectric. Comb drive actuation has several advantages: low power consumption, high speed, moderate driving voltage, low cost, high accuracy, and small form factor. For these reasons, 12 sets of comb, each with 42 electrodes, have been employed to operate the stretcher. In order to improve the stability of the actuation a ground plane has been created under the combs. The actuation force of a comb drive actuator is

$$F = N\varepsilon t V^2 / g \tag{4}$$

where N is the number of comb electrodes, ε is the dielectric permittivity of the surrounding medium, t is the comb electrode thickness, g is the comb electrode gap and V is the driving voltage [19]. According to this analytical model, the comb actuator exerts 60 μN with a driving voltage of just 100 V, when operated in air.

FEA has been carried out using a commercial software (Femlab 3.0), assuming plane stress and stress-strain linearity conditions. The undeformed and deformed mesh are presented in Figure 3, where the deformed shape has been obtained substituting the action of the comb drive with an equivalent load of 60 μN.

2.2 Fabrication of the MEMS

The design process is strongly dependent on the choice of the manufacturing technology, which limits the designer's options both from the geometrical standpoint and with respect to the available building materials. In order to keep the costs as low as possible and to increase the reliability and repeatability of the fabrication step, it has been decided to take advantage of the well-proven, commercial MUMPS foundry process (an excellent tutorial on the MUMPS process is downloadable from www.memscap.com). In essence the process is a Silicon-on-insulator method which starts from an n-type (100) silicon wafer. The wafer is futher n-doped using PoCl3 to stop charge feedthrough from the device to the single crystal silicon surface. Subsequently the Si3N4 insulator layer is deposited via low pressure chemical vapor deposition (LPCVD), followed by an analogous deposition of polycrystalline silicon (PolyS 0). This layer is then patterned by photolithography that is deposition of a photoresist, exposure through a mask and development of the photoresist to transfer the features of the mask to PolyS which is then etched with Reactive ion etch (RIE). Then surface is coated with a phosphosilicate glass (PSG) sacrificial layer patterned with dimples to provide anchor to the subsequent polycrystalline silicon (PolyS 1), 2 mm thick. Then another PSG layer is deposited and the whole wafer is annealed at 1050°C for 1 hr. Next PolyS 1with its top PSG is patterned and the PSG serves as a hard mask for the underlying PolyS 1. Basicly the process then repeats itself from the step of deposition of PSG till another

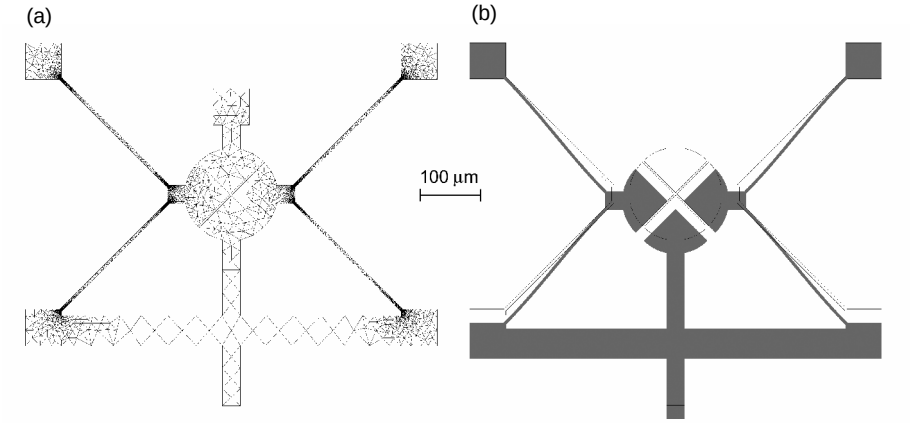

Figure 3: Meshed FEA model of the cell stretched platform (a), and deformed FEA shape plot (b).

Polycristalline silicon layer (PolyS 2) is deposited, patterned and etched.

Finally gold contacts are deposited on top. If MEMS are produced by commercial foundries, they are shipped to final users at this stage, protected by a polymeric coating of photoresist that must first be stripped by the final user by simple immersion in acetone and subsequent rinse in deionized water. Then the final release of the device must be performed by removing the sacrificial PSG layers. Two procedures have been used, differing in the concentration of HF: low (40% by volume in water) and high (49% by volume in water). In both cases the release was performed at room temperature for 1-2 minutes; the MEMS must then be washed in deionized water for 10 minutes, followed by immersion in ethanol to minimize static friction (stiction) and drying in oven at 110°C for 10 minutes. The MUMPS process provides also another method to reduce the problem of stiction, allowing the user to add dimples between the PolyS 0 and PolyS 1 layers. This is a very advisable technique, that has been used extensively during the platform design.

In order to drive the MEMS, electrical wires must be connected to the metal pads, which is usually obtained through wire bonding. This has been done after positioning and gluing the device on a proper support by means of a cyanoacrilate glue, thus obtaining a monolithic structure easy to manipulate. A home built printed circuit board (PCB) has been chosen as the support, in order to avoid the use of an expensive and not customizable commercial chip-carrier. In order to promote the adhesion of the thin aluminum wires (10 μm in diameter), the PCB contact electrodes have been coated by means of a simple galvanic cell with a thin layer of gold.

2.3 Experimental setup

To operate the MEMS statically in air, a simple DC power supply has been wired to the support plate connectors. Since comb drives are equivalent, from an electrical point of view, to ideal capacitors, they are able to operate at DC conditions without drawing energy from the power supply:

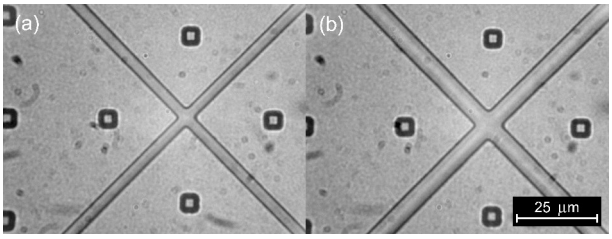

Figure 4: MEMS micrographs at different voltages

in fact the circulating current is effectively zero if the surrounding medium is an insulator, as in this case. This allows us to use a low-power, high output impedance power supply, composed of a high voltage generator in series with a voltage divider with a total resistance of 10 MΩ. The latter has been realized by means of a highly sensitive potentiometer, whose center tap has been directly connected to the comb drive stator. Using a high voltage generator it is possible to collect displacement informations, while reading the actual voltage by means of a high input impedance multimeter. To observe and record the MEMS behaviour, it has been placed on the stage of an optical microscope (Nikon Optiphot, 50x objective) equipped with a digital camera (Nikon Coolpix 4500), taking snapshot while the voltage has been increased stepwise from 0 to 100 V. Distances between opposite tips at different voltages has been calculated from the micrographs using a commercial image processing software (Matlab® Image Processing toolbox).

The experiments of the same device underwater have been performed applying a small drop of deionized water over the entire surface of the chip and covering it with a microscope slide glass window. In order to overcome electrolysis, that unavoidably would lead to device failure due to bubbling, an AC driving system has been employed [15]. It consists of a signal generator, that has been set to drive the comb with a 1 MHz square wave signal with an average voltage of 0 V. The rapid alternation of the position of anode and cathode inhibits a net development of gas at either electrodes, thus allowing the device to work properly for a prolonged time. Since the frequency response of the mechanical device drops rapidly at frequencies well below that of the input signal, and since the ideal transfer function of the comb drive depends on the square of the applied voltage, a net motion can be obtained, virtually with no traces of the high frequency carrier signal. As expected, since the relative permittivity of pure water is about 80, a great enhance in the displacement per volt has been observed, thus allowing to use driving voltages as low as 10 V peak-to-peak. A power amplifier has proven to be unnecessary, since the relatively high impedance of the equivalent capacitor of the comb drive allows the use of the signal generator without concerns about overloading (this is the result of the\ low capacitance value of the equivalent capacitor). The recording of the experimental data has been done with the same optical equipment already described, with the support of an oscilloscope for the acquisition of the effective amplitude signal.

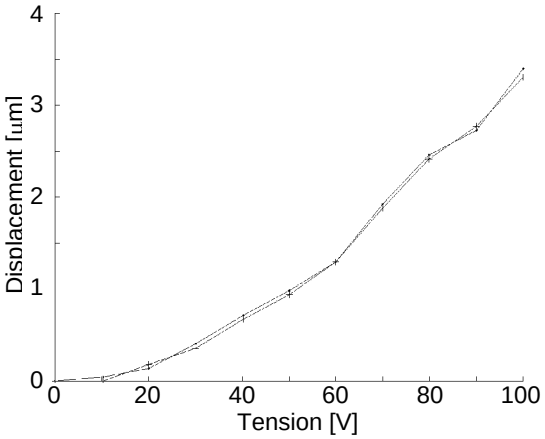

Figure 5: Plot of the stretcher platform displacement vs. driving voltage, in air.

3 RESULTS AND DISCUSSION

Figure 4 shows two optical micrographs of the circular platform center portion, respectively with 0 V (a) and 100 V (b) driving voltages, when the device is operated in air. It can be noticed that the distance between the two horizontal tips is approximately the same of the one between the vertical tips, which is in accordance with the initial assumptions about the kinematic behaviour of the mechanism.

Several tests show also the complete recovery of the initial position after removal of the applied voltage, which indicates the absence of any mechanical hysterysis.

A complete set of pictures has been acquired at different increasing voltages. Results are reported in plot of Figure 5. The curve is parabolic, because of the quadratic dependence of displacement on voltage [20].

Figure 6 represents the index of biaxiality, defined as

$$e = (\Delta x - \Delta y)/\Delta x \qquad (5)$$

versus Δx. For small displacements (lower than 1 μm) the error is high because of quantization errors due to low resolution of the camera device (the precision error of the vision system is 0.05 μm). On the contrary, for high displacements (higher than 3 μm), the error, which is not affected by vision system quantization errors, reaches a positive value of 5 %. The positiveness of the error is in accordance with the kinematic behaviour of the equivalent mechanism (see Figure 2). Nevertheless, the authors believe that an error of 5% is acceptable in order to produce a symmetric biaxial stress.

Figure 7 shows two optical micrographs of the device operating in deionized water, with 0 V and 20 V driving voltages, respectively.

The vertical (and horizontal) displacement is about 0.8 μm at 20 V. Such a value is higher than the one it has been measured in air at the same voltage, which is around 0.15 μm. This is reasonable since the water permittivity constant is 80 times higher than the air one. As the matter of fact the underwater displacement is lower than one would expect, which should be around 80 times the displacement in air, namely 80 x 0.15 = 12 μm. Such an undesired behaviour can be explained by the fact that water is prevented from flowing under the PolyS 1 layer, since its silicon-water interface tension is too high, causing the silicon surface to become hydrophobic [20]. Therefore resulting stiction forces across water-air meniscus reduce device performances. The hydrophobicity can be deduced by the spherical shape of water drops over the device.

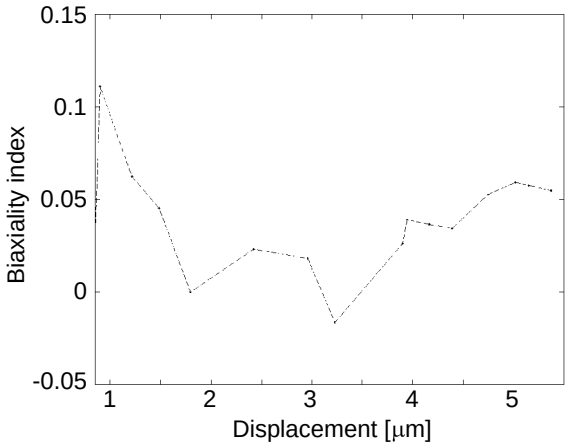

Figure 6: Biaxiality index vs. displacement.

In order to avoid this problem, the silicon-water interface tension has been reduced by adding a surfactant (soap) solution until the silicon surface becomes hydrophilic.

4 CONCLUSIONS

A novel MEMS platform whose perspective applications include the characterization of the mechanical properties of biaxially loaded living cells has been designed and the mask files sent to foundry for manufacturing. Despite the remarkable economical advantages of using a commercial microfabrication route, the choice of the MUMPS technology posed many constraints to the design process. Despite of this, by proper design and optimization, the resulting device has been successfully put into operation and the single-actuator biaxial stretcher principle has been positively verified in air. It is also interesting to note that by proper functional simulation and by a process-oriented design strategy, it has been possible to obtain an acceptable behaviour of the devices since the first foundry run.

The same experiments have been repeated with the device submersed in deionized water. Electrolysis has been effectively avoided by means of high frequency drive, also in long-term tests. As expected, the hydrophobicity of the silicon-water interface caused air trapping between the comb drive teeth and the MEMS baseplate, thus reduction the effective efficiency of the electrostatic system well below the expected value. In fact, a slight increase in the displacement per volt has been observed, but not high enough to fit the theoretical values due to the high value of the relative permittivity of water. In order to overcome this problem, a surfactant has been added to the deionized water. However, a net decrease in the total displacement has been observed. This behaviour can be attributed to the increased conductivity of the resulting solution, which poses severe problems of electrical conduction due also to the small gap between adjacent teeth.

The developed platform will hopefully open new perspectives in the field of mechanical characterization of

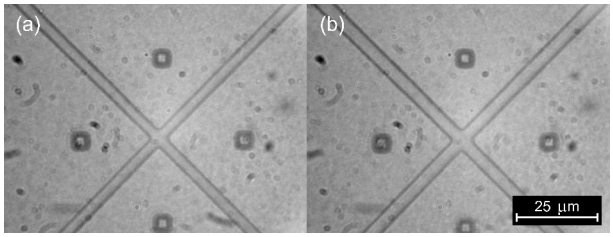

Figure 7: Underwater MEMS behaviour

living cells of great significance for the human life, e.g. that belonging to the pericardium, which are mainly subjected to biaxial stretching loads. As a future work, it is planned to explore new possibilities for what concerns the control of the efficiency of underwater comb drive actuators, like the system reworking by means of suitable surfactants and surface functionalization systems. Moreover, the biocompatibility of the stretcher platform surface will be increased by the deposition of a proper coating by means of a micropatterning system.

REFERENCES

[1] Fung YC, Biomechanics: mechanical properties of living tissues 2nd ed. Springer NY, 1993.

[2] Fung YC, Biomechanics: Motion, Flow, Stress and growth, Spinger, NY 1990.

[3] Fung YC, Biomechanics: circulation 2nd ed. Springer NY, 1997.

[4] Somjen D, Binderman I, Berger E, Harrel A. Biochimica and Biophisica acta 1980; 627:91-100.

[5] Jones DB, Nolte H, Scholuebbers JG, Turner E, Veltel D. Biomaterials 1991; 12:101-110.

[6] Neidlinger-Wilke C, Wilke HJ, Claes L. Journal of orthopaedic research 1994; 12:70-78.

[7] Andersen KL, Norton LA. A device for the application of known simulated orthodontic forces to human cells in vitro. Journal of Biomechanics 1991; 24:649-654.

[8] Bottlang, M, Simnacher M, Schmitt H, Brand RA, Claes L. A cell strain system for small homogeneous strain applications. Biomedizinische Technik 1997; 42: 305-309.

[9] Brighton CT, Strafford B, Gross SB, Leatherwood DF, Williams JL, Pollack SR. The proliferative and synthetic response of isolated calvarial bone cells of rats to cyclic biaxial mechanical strain. Journal of Bone and Joint Surgery 1991; 73A:320-331.

[10] Brighton CT, Sennett BJ, Farmer JC, Iannotti JP, Hansen CA, Williams JL, Williamson J. The inositol phosphate pathway as a mediator in the proliferative response of rat calvarial bone cells to cyclical biaxial mechanical strain. Journal of Orthopaedic Research 1992; 10:385-393.

[11] Bucklely MJ et al. Osteoblasts increase their rate of division and align in response to cyclic, mechanical tension in vitro. Bone and Mineral 1988; 4:225-236.

[12] Harell A, Dekel S, Binderman I. Biochemical effect of mechanical stress on cultured bone cells. Calcified Tissue Research 1977; 22:202-207.

[13] Hung CT, Williams JL. A method for inducing equi-biaxial and uniform strains in elastomeric membranes used as cell substrates. Journal of Biomechanics 1994; 27:227-232.

[14] Deutsch J, Motlagh D, Russell B, Desai TA. Fabrication of microtextured membranes for cardiac myocyte attachment and orientation. Journal of Biomedical Materials Research 2000; v 53, 3: 267-275.

[15] Sounart TL, Michalske TA. Electrostatic actuation without electrolysis in microfluidic MEMS. TRANSDUCERS '03 - The 1Bh International Conference an Solid Slate Sensors, Actuators and Microsystem Boston, June 8-12, 2003.

[16] Sotoudeh M, Jalali S, Usami S, Shyy JY-J, Chien S. A Strain Device Imposing Dynamic and Uniform Equi-Biaxial Strain to Cultured Cells. Annals of Biomedical Engineering 1998; 26:181–189.

[17] Barbee KA, Thibault LE. Strain Measurements in Vascular Smooth Muscle Cells Grown on a Biaxially-Stretched Substrate. IEEE Engineering in Medicine & Biology Society - llth Annual International Conference ANNUAL INTERNATIONAL CONFERENCE, 1989.

[18] Toupin RA, Saint Venant's principle, Spinger-Verlag, NY 1965.

[19] Chihchung C,Chengkuo L, Yen JL, Wenchih C, Development and Application of Lateral Comb-Drive Actuator, Jpn.J.Appl.Phys 2003, 42, 4059 – 4062.

[20] Sameoto D, Hubbard T, Kujath M, Operation of electrothermal and electrostatic MUMPs microactuators underwater, J. Micromech. Microeng. 2004, 14, 1359–1366.